Enhancement in the Antibacterial Activity of Rifaximin by Delivery through Gelatin Nanoparticles

Nida Iqbal,[a] Amber Bano,[b] Daim Asif Raja,[a] Ali Raza,[a] Rabia Ilyas,[c] Rafia Akhlaq,[c] Imran Saleem,[d] Ayaz Ahmed,[c] Syed Ghulam Musharraf,[a,c,**] Muhammad Imran Malik[a,b,*]

[a] H.E.J. Research Institute of Chemistry, International Center for Chemical and Biological Sciences, University of Karachi, Karachi, 75270, Pakistan
[b] Third World Center for science and technology, International Center for Chemical and Biological Sciences, University of Karachi, Karachi, 75270, Pakistan
[c] Dr. Panjwani Center for Molecular Medicine and Drug Research, International Center for Chemical and Biological Sciences, University of Karachi, Karachi, 75270, Pakistan
[d]School of Pharmacy &BiomolecularSciences, Liverpool John Moores University, UK

Email: *mimran.malik@iccs.edu; **musharraf1977@yahoo.com

Abstract:

Objectives: Bacterial infections are a noteworthy global health concern that necessitates the development of new strategies to enhance the potency and efficacy of antibiotics. Rifaximin (RFX), a broad-spectrum antibiotic, exhibits promising antibacterial activity against several bacterial strains. However, its insolubility and impermeability impede the exploitation of its full potential. The objective of the current study is to overcome the inherent caveats of RFX in order to exploit its maximum potential.

Significance: The exploitation of the full potential of antibiotics is necessary for reduction in their dosage and to minimize antibiotic pollution. This is a preliminary study aiming for maximum utilization of RFX at the target site and reduction in its release in unmetabolized form.

Methods: Gelatin is a biopolymer that has gained significant attention for biomedical applications owing to its inherent biocompatibility and biodegradability. In this study, bovine gelatin nanoparticles (BGNPs) were fabricated by the self-assembly method for their application as a carrier of RFX to enhance its antibacterial activity. The study employs a comprehensive range of experimental techniques to characterize the fabricated BGNPs such as DLS, Zeta Potential, FT-IR, AFM, SEM-EDX, and UV-Vis spectrophotometry.

Results: The average size of the fabricated BGNPs was 100 nm with a zeta potential value of -15.3 mV. The loading of RFX on BGNPs rendered an increase in its size to 136 nm with a zeta potential value of -16 mV. *In-vitro* assays and microscopic analyses were conducted to compare the antibacterial efficacy of RFX and RFX@BGNPs. An excellent loading capacity followed by sustained release of RFX from RFX@BGNPs rendered a significant enhancement in its pharmaceutical efficacy. The release of RFX from

RFX@BGNPs followed the Higuchi and Korsmeyer-Peppasmodels. The antibacterial efficacy of RFX against *Staphylococcus aureus* has doubled by delivery through RFX@BGNPs, assessed by inhibitory and biofilm inhibitory assays. The enhancement in the antibacterial efficiency was further endorsed by SEM and microscopic imaging of the control and treated bacterial colonies.

Conclusion: The study demonstrates an enhancement in the antimicrobial efficacy of RFX by its delivery in the form of RFX@BGNPs to exploit its full potential for practical applications.

Keywords: Rifaximin (RFX); Bovine gelatin nanoparticles (BGNPs); *Staphylococcus aureus;* RFX@BGNPs.

1. Introduction

Bacterial infections are one of the leading global health issues that significantly contribute to the occurrence of severe illnesses, which may ultimately lead to death [1]. Numerous pathogenic bacterial species, such as *Mycobacterium spp., Staphylococcus aureus, Listeria monocytogenes, Escherichia coli,* and *Brucella spp. etc.* are responsible for this huge negative impact on human life. Antibiotics have historically been used to treat bacterial infections [2]. However, the associated inherent limitations of antibiotics hinder access to their full potential, for instance, consistently increasing antibiotic resistance due to their excessive utilization, limited bioavailability of the drug at the target site owing to their low solubility and permeability, and so on [3]. Hence, new strategies to combat microbial infections are required, and nanotechnology could help in the targeted and sustained delivery of drugs to the infected site [4]. Nanoparticles (NPs) have been employed to improve the targeted delivery and, in turn, the efficacy of various therapeutic agents [5]. The advantages associated with NP-based drug delivery systems compared to conventional dosage formulations include enhanced solubility, bioavailability, and efficacy of the drug along with the reduction in its toxicity [6].

Rifaximin (RFX), a semi-synthetic derivative of rifamycin, is synthesized by reaction of 2-amino-4-methylpyridine with rifamycin O (the oxidized form of rifamycin B) [7]. It is a broad-spectrum antibacterial agent against both Gram-positive and Gram-negative bacteria. It functions by inhibiting the bacterial protein synthesis through its action on the DNA-dependent RNA polymerase enzyme [8]. According to the Biopharmaceutics Classification System (BCS), RFX belongs to class IV antibiotics that are associated with low water solubility. However, it has good solubility in organic solvents such as DMSO (about 10 mg/mL), DMF, and ethanol (about 30 mg/mL). Because of its poor solubility in water, its effective daily therapeutic dose ranges from 600 mg to 800 mg. The limited aqueous solubility and low permeability of

RFX, similar to all BCS class IV drugs, are the major challenges affecting its therapeutic efficacy [9]. RFX is a non-systemic drug that is neither absorbed nor inactivated in the gastrointestinal tract (GIT) [10]. Furthermore, *in vivo* studies demonstrate that the gastrointestinal absorption of RFX following oral administration is rather low, less than 0.4% of the administered dose [11]. Due to RFX's distinct capacity as a non-absorbable drug, it remains in high concentrations in the gastrointestinal lumen [12]. It can effectively treat various gastrointestinal diseases without having significant adverse side effects on the rest of the body. Hence, it is a promising candidate for preventing bacterial activity, especially of *staphylococcus aureus* in the small intestine [13], and is designated as a gastrointestinal-specific drug for enteric pathogens [14]. RFX exhibits a strong antibacterial activity against extracellular *staphylococcus aureus* [15]. However, it is ineffective for the treatment of intracellular *S. aureus* infections due to its low permeability [16]. Numerous challenges that potentially reduce its therapeutic efficacy include water insolubility, weak intracellular permeability, and limited systemic absorption. To overcome these constraints and improve its therapeutic efficacy, various drug delivery systems have been proposed such as chitosan nanoparticles [17], chitosan nanogels [15], and cyclodextrins [18] etc. Targeted drug delivery systems are important because of their ability to deliver drugs to the desired site to improve their efficacay and reduce the associated side effects.

In this context, gelatin, a natural biopolymer, obtained by the hydrolysis of collagen, has emerged as an attractive candidate for drug delivery applications [19]. It has gained significant attention in pharmaceutics and medicine due to its inherent biocompatibility and biodegradability in physiological environments [20]. Gelatin has low antigenicity and is approved by the Food Development Administration (FDA) for safe extravascular administration [21]. Improved efficacy of drugs by their delivery through Gelatin nanoparticles (GNPs) has been demonstrated for numerous drugs, such as doxorubicin [22], moxifloxacin [23], amphotericin B [24], resveratrol [25] etc. Several techniques have been used for the fabrication of GNPs, for instance, freeze-thaw method [26], nanoprecipitation [27], two-step desolvation [28], and self-assembly method [29,30]. Cascone et al. reported that gelatin nanoparticles produced by w/o emulsion method had a methotrexate loading efficiency of 5.6–15.6% [31]. Utilizing the same method, a loading efficiency of 15–19% was obtained for chloroquine phosphate [32]. The coacervation method was used to prepare GNPs that have a loading efficiency of 30–50% for various drugs [22]. Moreover, 7.1–18.5% loading for cycloheximide was obtained for the GNPs prepared by a two-step desolvation method [33]. Hence, the loading efficiency of GNPs prepared by different methods substantially differs for different drugs.

The major barrier for drug delivery applications of GNPs is their large size (>200 nm) due to inconsistent molecular weight of pristine gelatin [34]. Although GNPs with a size range of 150-300 nm have been

prepared through the traditional desolvation method, the fabricated GNPs are unstable and tend to aggregate [13]. This study aims to explore the maximum loading of RFX, a hydrophobic antibiotic, in GNPs produced by the self-assembly method using glutaraldehyde as a crosslinker [29,30].

In this study, we fabricate Bovine Gelatin Nanoparticles (BGNPs) to be employed as a carrier for Rifaximin (RFX) for improvement its solubility and delivery to the target site. The BGNPs were prepared using the self-assembly method that rendered BGNPs of small size and narrow dispersity (PDI). The thermal stability of BGNPs was evaluated via thermogravimetric analysis (TGA), while atomic force microscopy (AFM) and scanning electron microscopy (SEM) were employed to examine their surface morphology. Furthermore, the interaction of functional groups of BGNPs with RFX and their loading capacity were investigated using Fourier transform infrared (FT-IR) and UV-visible spectroscopy, respectively. The RFX@BGNPs were then evaluated for different critical biological parameters that include the cumulative release of RFX, cytotoxicity evaluations to ensure their safety for potential use in living systems, and antibacterial activity to evaluate their efficacy in combating bacterial infections. In essence, the biological segment of our study demonstrates the significant potential of BGNPs as a versatile drug delivery system for improvements in therapeutic outcomes and combating bacterial infections.

2. Materials and Methodology

2.1. Materials

Gelatin standard (Bovine), CAS # 9000-70-8, was purchased from LeapChem, China. Glutaraldehyde grade 1 (25% v/v aqeuous solution), and methanol HPLC grade were purchased from Honeywell company, Germanywhile Sodium metabisulphite ($Na_2S_2O_5$) was procured from Sigma Aldrich, United States. Sodium hydroxide was supplied from Uni-chem, Indiawhile hydrochloric acid was purchased from Merck, Germany. RFX was provided by a local pharmacy. All solvents were of analytical grade. The fibroblast cell line BJ(CRL-2522) was purchased from American Type Cell Culture (ATCC). The Dulbecco's Modified Eagle Medium (DMEM) and transparent flat-bottomed 96-well plates from Sigma Aldrich, United States were used in cytotoxicity experiments. Millipore water with a resistivity of 18.2 MΩ·cm was used for all the experiments.

2.2. Preparation of Bovine Gelatin Nanoparticles (BGNPs)

Bovine gelatin was dissolved in milli-Q water at 50 °C maintaining a concentration of 10 mg/mL. The solution of gelatin was filtered to remove undissolved gelatin particles. The pH of the bovine gelatin

solution was adjusted to 11 by 0.1 M NaOH solution followed by the dropwise addition of 25% glutaraldehyde at room temperature. Self-assembly of gelatin was triggered by cooling the solution that results in the formation of GNPs. BGNP solution was further stirred magnetically at 500 rpm for 3 hrs to attain uniform distribution of glutaraldehyde and cross-linking among gelatin molecules. Finally, sodium metabisulphite was added to remove unreacted glutaraldehyde.

2.3. Loading of RFX on BGNPs

RFX loading on BGNPs was conducted using the encapsulation technique [35]. The procedure of BGNP preparation was performed as stated in Section 2.2 followed by the addition of 200 µL of RFX (2.5 mg/mL in methanol). Finally, glutaraldehyde was added to crosslink the prepared BGNPs.

2.4. Characterization of BGNPs and RFX@BGNPs

2.4.1. Particle Size and Zeta Potential

Fabricated BGNPs and RFX@BGNPs were characterized using DLS (Zetasizer Nano, Malvern Instruments Ltd. United Kingdom) for average mean size and zeta potential.

2.4.2. Morphological Analysis by AFM and SEM

Morphological features of BGNPs and RFX@BGNPs were examined by Scanning Electron Microscopy (SEM), Thermo Fisher Scientific, USA. Lyophilized samples were coated on gold-coated aluminum stubs before analysis. Atomic Force Microscope (AFM), Agilent Technologies 5500, Arizona, USA, was employed for topographic imaging. Initially, samples were prepared by adding 10 µL of sample on mica sheets that were air-dried before analysis.

2.4.3. Fourier Transform-infrared Spectroscopy (FT-IR)

FTIR analyses of RFX, glutaraldehyde, bovine gelatin, BGNPs, and RFX@BGNPs were performed by direct sampling using the ATR-FTIR spectrometer equipped with single reflectron diamond (Thermoscientific, model iS-50 Nicollet) in a range of 500 cm^{-1} to 4000 cm^{-1} at 25 °C.

2.4.4. Thermogravimetric analysis (TGA)

Thermal properties of BGNPs and RFX@BGNPs were evaluated by TGA on a TGA-Q-50-TA instrument, USA, in a temperature range of 30-650 °C at a heating rate of 20 °C per min under nitrogen atmosphere.

The sample (5-10 mg) was taken and weight loss of the sample as a function of increase in temperature was recorded [36].

2.4.5. Drug-loading Capacity

The entrapment efficiency of BGNPs for RFX was investigated by UV-visible spectroscopy (Shimadzu double beam spectrophotometer, UV-1800 series). RFX-loaded BGNPs were centrifuged at 14000 rpm for 15 min. The supernatant was collected to determine the free amount of RFX by measuring its absorbance at 450 nm. The remaining RFX in the supernatant was determined by using a calibration curve of RFX. Drug-loading of RFX was calculated by the formula

$$Drug\ loading\ (\%) = \frac{Total\ drug\ used - Free\ drug}{Total\ drug\ used} \times 100$$

2.4.6. *In-vitro* Release Study

The *in-vitro* release of RFX from BGNPs was performed in 2 mL phosphate buffer saline (PBS) for 24 hrs at 37 °C in a thermoshaker shaking at 300 rpm. RFX@BGNPs pellet was weighed (4.06 mg) and redispersed in PBS by shaking at 10,000 rpm. At fixed intervals of 15 mins, 0.5 mL sample was withdrawn and replaced by fresh PBS to maintain the volume. The supernatant was analyzed by UV-Vis spectrophotometer for the amount of released RFX [25].

2.4.7. Kinetics Models

To evaluate the mechanism of drug release and kinetics, *in-vitro* drug release data of RFX from RFX@BGNP was tested against five kinetic models using DDSolver program. The equations of the kinetic models are presented in Table 1.

Table 1

Model	Equation
zero-order	$F = k_0 \times t$
First order	$F = 100 \times [1 - e^{(-k_1 \times t)}]$
Higuchi	$F = K_H \times t^{0.5}$
Hixson-Crowell	$F = 100 \times [1 - (1 - K_{HC} \times t)^3]$
Korsmeyer-Peppas	$F = K_{KP} \times t^n$

Where F is the fraction(%) of drug released in time t, k_0 is the zero-order release constant, k_1 is the first-order release constant, k_H is the Higuchi release constant, k_{HC} is the release constant in Hixson–Crowell

model, and k_{KP} is the release constant of Korsmeyer-Peppas model while 'n' is the diffusional exponent indicating the drug-release mechanism.

2.5. Biological Studies

2.5.1. Cytotoxicity of BGNPs and RFX@BGNPs

BJ fibroblast cells were seeded in 96-well culture plates (2,500 cells/ well) and incubated for 24 hrs at 37 °C. On the second day of incubation, BGNPs and RFX@BGNPs were added to serum-free media in concentrations ranging from 150 µg/mL to 4.68 µg/mL using a trifold dilution in triplicates to determine individual IC_{50} doses of BGNPs and RFX@BGNPs [37]. After 24 hrs, cell viability was measured by 3-(4,5-dimethylthiazol-2-yl)-2, 5-diphenyl tetrazolium bromide (MTT) dye, and absorbance was measured at 570 nm using a spectrophotometer (Thermo Scientific Multiskan GO). IC_{50} doses of tested compounds were normalized to untreated control samples and the dose-response inhibition curve [log (inhibitor) *vs*. normalized response] was generated using GraphPad Prism V.

2.5.2. Antibacterial Activity

The Minimum Inhibitory Concentration (MIC) is defined as the lowest concentration that inhibits the growth of bacteria [38]. The MIC was determined using the broth micro-dilution method to determine the lowest effective concentration of BGNPs, RFX@BGNPs, and RFX against *Staphylococcus aureus*(ATCC-25293).

$$Inhibition\ (\%) = \frac{OD\ of\ control - OD\ of sample}{OD\ of\ control} \times 100$$

2.5.3. Bacterial Growth Inhibition Assay

The antibacterial activity of the RFX, BGNPs, and RFX@BGNPs was determined as minimum inhibitory concentration (MIC) using a micro-titer broth dilution assay. The assay was performed on a 96-well plate (Nest, China). RFX and RFX@BGNPs were diluted two-fold serially from the 1st well to the 9th well, the concentration of compounds was in the range of 11.2 µg/mL to 0.025 µg/mL. After preparing compound dilutions, 10 µL bacterial inoculum ($5x10^5$ cfu/mL) was added in each well except negative control wells. Each lane contains positive control (media plus bacterial culture), solvent control, and negative or sterility control (only media) [39]. The final volume in each well was maintained at 200 µL. After preparation, the

plate was incubated overnight at 37 °C. MIC was calculated as the lowest dose that inhibited bacterial growth after 24 hrs.

2.5.4. Minimum Biofilm Inhibitory Concentration (MBIC)

The inhibition of biofilm formation was assessed by the MBIC. The Minimum Biofilm Inhibitory Concentration (MBIC) is defined as the lowest concentration of antibiotics that inhibit biofilm viable cells[40]. The crystal violet assay method was employed to determine the minimum biofilm inhibitory concentration of RFX and RFX@BGNPs. The plate was set as mentioned in the antimicrobial assay and the next day the spent media was decanted and washed thrice to remove non-adherent cells. The attached biofilm was stained with 0.1% crystal violet dye for 10 min. The stain was decanted, and wells were gently washed with tap water to remove excess dye followed by heat fixing for 45 min. The stain was dissolved in 200 µL of 30% (v/v) glacial acetic acid and absorbance was measured at 590 nm. The lowest concentration that inhibited 50% of biofilm was considered the minimum biofilm inhibitory concentration (MBIC) [41]. The 48-well plate was observed under a light microscope at 0.5 x MIC, MIC, and 2 x MIC concentrations along with positive and negative controls.

2.5.5. Time Kill Assay

A time-kill assay was performed to determine the time point of the RFX and RFX@BGNPs at which they start to inhibit bacterial growth [42] *S.aureus* (5×10^5 CFU/mL) was treated with RFX and RFX@BGNPs at 0.5 x MIC, MIC, and 2 x MIC concentrations, and placed in a spectrophotometer with an incubator at 37 °C for 24 hrs. The plate also has positive and negative controls. During incubation, the absorbance of the wells was read at 600 nm and recorded at an interval of 1 hr, i.e., 0, 1, 2, 3, 4, 5, 6, and 24 hr. The assay was performed in triplicate, and OD values were plotted against time to determine the time when RFX and RFX@BGNPs stop inhibiting bacterial growth.

3. Results and Discussion

Bovine gelatin nanoparticles (BGNPs) are fabricated by self-assembly method through optimization of the concentration of gelatin, amount of glutaraldehyde, pH, and temperature [29]. The concentrations of gelatin and glutaraldehyde were the major factors influencing the size of the BGNPs. Figure 1 demonstrates the selectivity of different experimental parameters for the size of BGNPs. The particle size increased with the increase in the gelatin concentration from 5 to 20 mg/mL while keeping other variables at their optimum (25 % glutaraldehyde solution: 50 µL; temp.: 50 °C; pH: 11), Figure 1A [43]. The particles using higher

concentrations of gelatin have a PDI of 0.2 indicating a fair uniformity of the synthesized BGNPs. Thus, 10 mg/mL is taken as an optimum concentration of gelatin for further experimentation. On the same line, the amount of 25% glutaraldehyde solution is varied from 30-60 µL while keeping other parameters at the optimum (amount of gelatin:10 mg/mL; temp.: 50°C; pH: 11). The smallest average size of BGNPs is obtained while using 50 µL of 25% glutaraldehyde solution, which is taken as an optimum. Any increase or decrease in the amount of 25% glutaraldehyde solution rendered an increased size and dispersity, similar results were reported by Ofokansi et, al. [44], Figure 1B. On the same lines, the temperature was varied from 40 °C to 60 °C while keeping the remaining parameters at their optimum (amount of gelatin:10mg/mL; 25% glutaraldehyde solution: 50 µL; pH:11). Formation of gelatin nanoparticles was not possible at ambient temperature (25 °C) due to gel-forming property of gelatin. However, changes in the temperature from 40 °C to 60 °C had an impact on the size of the BGNPs, the smallest particles were obtained at 50 °C, Figure 1C. At 40 °C, gelatin still has a gelling tendency. At 50 °C, the helical structure seems to be completely uncoiled, leading to the formation of smaller particles. The increase of temperature to 60 °C increased the size of the particles, which can be attributed to the gelatin's triple helical structure that begins to uncoil at higher temperatures, causing a decrease in the viscosity [24,45].

Moreover, the effect of pH on the size, PDI, and zeta potential of the BGNPs is systematically evaluated, Figure 1D. Gelatin is a polyelectrolyte with low charge density, the net charge depends on the pH of the solution. The isoelectric point (IEP) of bovine gelatin is in the pH range of 4.7-5.2 [44]. The simultaneous presence of carboxylic acid and amine groups in gelatin makes it a versatile natural polymer that can be tailored and maneuvered for its applications by varying the pH of the medium. The stability of NP suspension critically depends on the surface charge repulsion. The surface charge of BGNPs is pH dependent, in the acidic range BGNPs have a positive surface charge while BGNPs have a negative surface charge in the basic range. An increase in the pH of the BGNP solution above the pKa value of the side chain of amino acid causes their deprotonation that renders an increase in the negative charge [46]. The size of BGNPs initially increased and subsequently decreased consistently with an increase in the pH of the medium [44]. The maximum obtained size of 290 nm at pH 5 can be attributed to the most coiled conformation of gelatin chains near their IEP [47]. The elongated state of BG that is present away from IEP facilitates the formation of BGNPs. The minimum size of 100 nm is achieved at pH 11. Hence, pH 11 is taken as the optimum for further experimentation that renders a size of 100 nm and a surface charge of -15.3 [24,44]. Hence, the overall optimum conditions for the synthesis of BGNPs are 10 mg/mL gelatin concentration, 50 µL of 25% glutaraldehyde solution, pH 11, and 50 °C temperature.

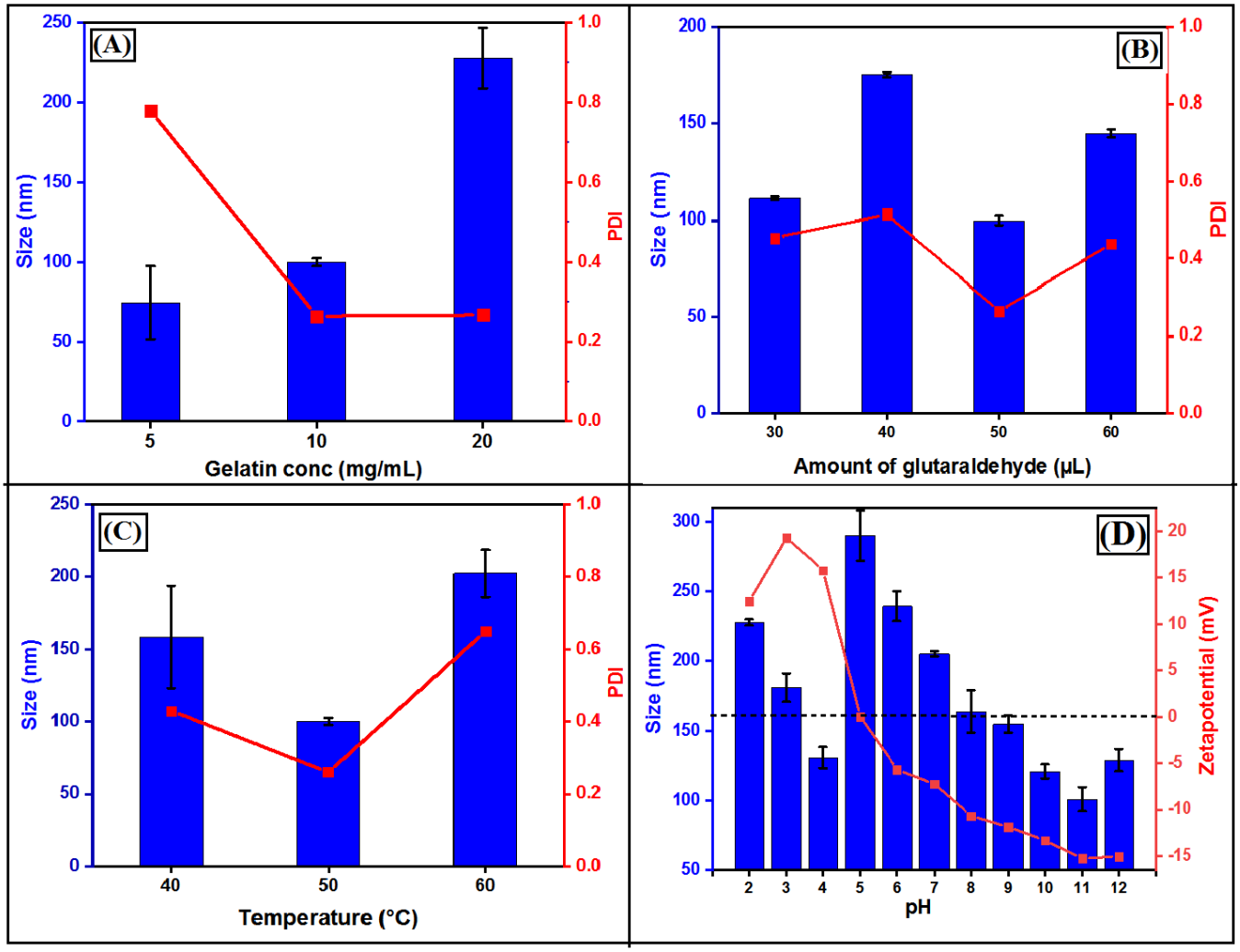

Figure 1

3.2. Loading of RFX onBGNPs

An important milestone towards the major goal of the study is the efficient loading of RFX on BGNPs. The efficiency of Bovine gelatin nanoparticles (BGNPs) as a rifaximin delivery system depends upon its particle size, zeta potential, morphology, and thermal stability. The interaction of RFX with BGNPs is endorsed by DLS, AFM, SEM-EDX, and zeta potential analysis of BGNPs before and after interaction with RFX. DLS clearly shows an increase in the mean size of BGNPs from 100 to 136 nm after interaction with RFX, compare Figure 2A-I and Figure 2B-I. Another important feature is the zeta potential value of BGNPs that confirms the stability of nanoparticles, it helps to keeps the particles apart and avoid aggregation. The value of zeta potential away from zero in either direction indicates the stability of the nanoparticles. The zeta potential values of BGNPs before and after the addition of RFX remained similar (-15.3 to -16.0 mV), Figure S1-supplementary material. An increase in the size of BGNPs after interaction with RFX is further endorsed by AFM and SEM analysis, compare Figure 2A-II&III with Figure 2B-II&III. AFM distribution

graph is presented in Figure S2-supplementary material. Moreover, an increase in carbon (%) while a decrease in nitrogen (%) and oxygen (%) content further confirms the loading of RFX on BGNPs, Figure S3-supplementary material.

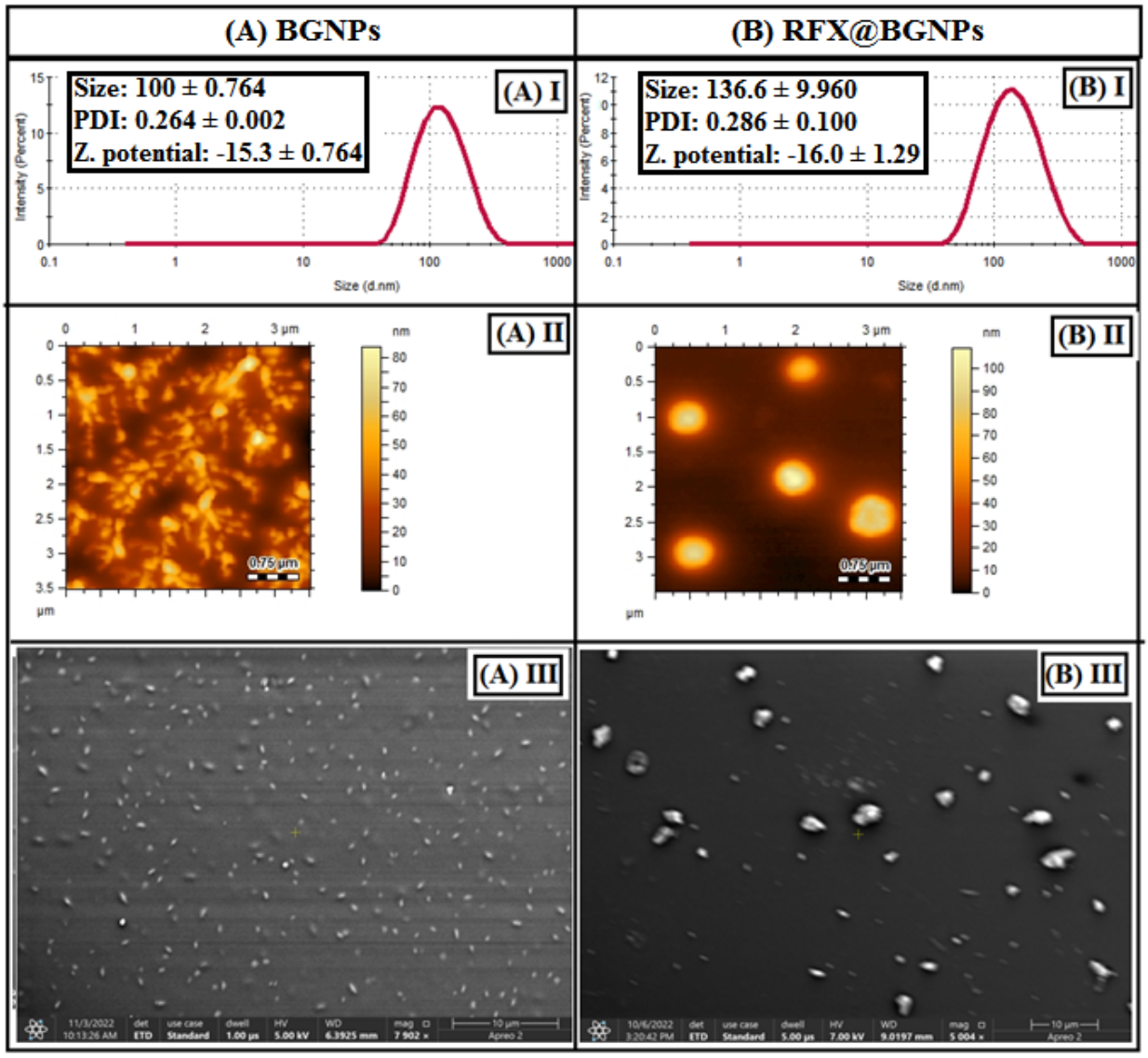

Figure 2

The TG-DTG thermograms of the Bovine Gelatin Nanoparticles (BGNPs) and Rifaximin-loaded Bovine Gelatin Nanoparticles (RFX@BGNPs) are presented in Figure S4-supplementary material. In this analysis, two primary thermal decomposition peaks are observed in the derivative thermogravimetry (DTG) with corresponding weight losses as noted in the thermogravimetric (TG) curve. The first DTG peak and associated weight loss, occurring at 60 °C, can be attributed to the removal of the moisture. The second and more prominent peak in the DTG curve is observed at 318 °C for BGNPs and 328 °C for RFX@BGNPs,

respectively. These peaks are associated with the mass loss corresponding to the decomposition of the gelatin backbone [36].

The initial weight loss in both BGNPs and RFX@BGNPs in the temperature range of 30 to 230 °C accounts for approximately 15% of the total, which may be attributed to moisture and the unreacted reagents. The major weight loss, constituting approximately 70-80% of the total, is observed in the temperature range of 230-600 °C for BGNPs and 230-650 °C for RFX@BGNPs [48]. The latter corresponds to the degradation of the BGNPs. Overall, there is no significant difference in the thermal degradation behavior of BGNPs and RFX@BGNPs.

FTIR spectrum of glutaraldehyde has characteristic absorption bands at 1716 cm^{-1} (stretching vibration of C=O), 2966 cm^{-1} (stretching vibration of C-H), and 3367 cm^{-1} (stretching vibration of O-H), Figure 3 [49]. Similarly, Bovine gelatin has characteristic absorption peaks at 3495 cm^{-1} (amide-A), 1650 cm^{-1} (amide-I), and 1531 cm^{-1} (amide-II) corresponding to the polypeptide conformation. The carbonyl (C═O) stretching vibration of the amide group is attributed to amide-I while amide-II is associated with NH bending and CN stretching vibrations. The other peak at 2940 cm^{-1} is due to the CH_2 stretching and bending [36]. There is a shift in amide-I and amide-II peaks to 1630 cm^{-1} and 1545 cm^{-1} from corresponding peaks in BG that indicates the BGNP formation. The carbonyl group of glutaraldehyde is involved in BGNP formation. Amide-A peak due to N–H stretching appeared at 3437 cm^{-1}, associated with the degree of cross-linking [26]. The RFX spectrum exhibits typical absorption bands at 1720 cm^{-1} (stretching vibration of C=O), 2985 cm^{-1} (stretching vibration of C-H), 2868 cm^{-1}(stretching vibration of C-C), and 3454 cm^{-1} (stretching vibration of O-H)[15]. Overall, RFX@BGNPs have a similar FT-IR profile as that of BGNPs and hydrogen bonding seems to be the major binding force, supported by the appearance of peaks at 1630 cm^{-1}, and 1529 cm^{-1} along with the disappearance of amide-A band (3500-3600cm^{-1}) [25].

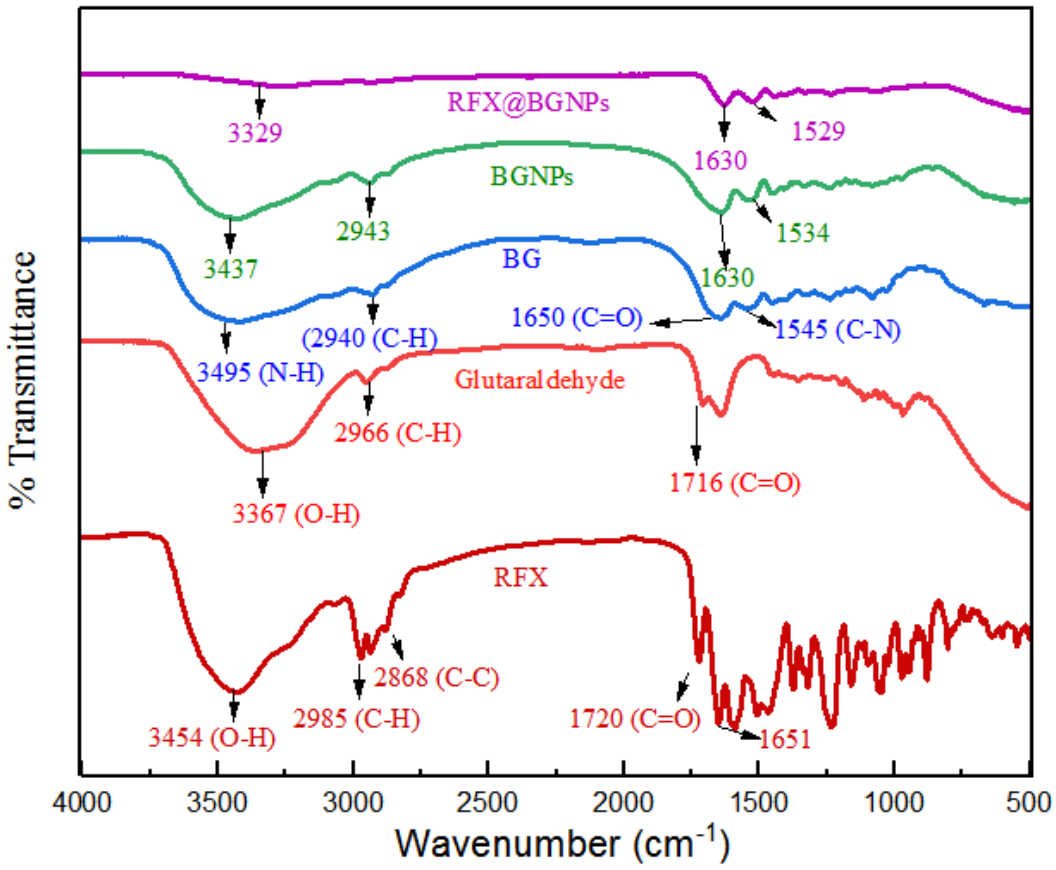

Figure 3

UV-Vis analysis of the supernatant revealed a reduction of 88% in the initial concentration of RFX after treatment with the BGNPs. In this context, the concentration-dependent spectra of RFX, having adsorption maxima at 440 nm, are presented in Figure S5A-supplementary material. The absorbance at 440 nm as a function of the concentration of RFX renders its calibration curve, Figure S5B-supplementary material. The developed calibration curve is used for the calculation of the remaining RFX in all experiments. Hence, the RFX entrapment efficiency of BGNPs is found to be 88%. The loading of Rifaximin on BGNPs is found to be higher compared to tamarind gum polysaccharide nanoparticles [50]. Moreover, the loading efficiency of the Fluorescein-Isothiocyanate (FITC)-Dextran loaded bovine gelatin nanoparticles was also lower compared to BGNPs reported in this study [43].

3.3. Release Behavior of RFX from BGNPs

The release behavior of the loaded RFX from BGNPs is presented in Figure 4. After about 40% of the initial burst in the first 2 hrs, there is a gradual decrease in the release extent leading to almost 95% release

in 24 hrs. The burst release was associated with the amount of drug bound on the surface of BGNPs while the drug entrapped in the matrices released gradually in a sustained manner [24,44].

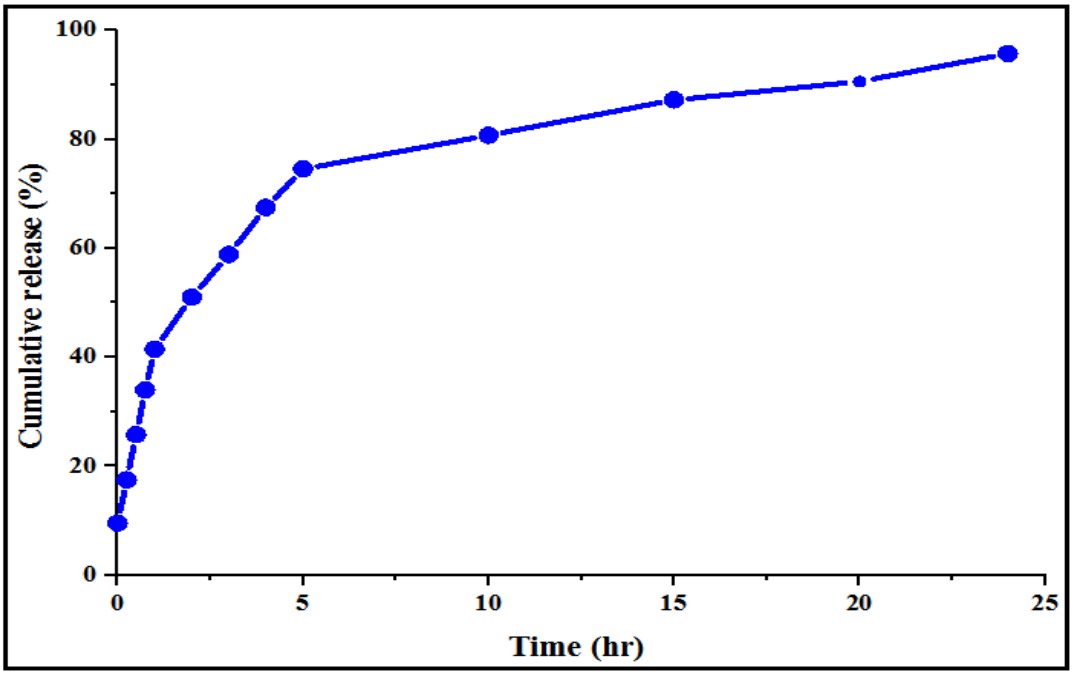

Figure 4

In order to understand the kinetics and release mechanism of RFX from BGNPs, the drug release data were fitted for various kinetic models, for instance, zero order, first order, Higuchi, Hixson-Crowell, and Korsmeyer-Peppal using DDSolver [51]. DDSolver provides a variety of statistical criteria to estimate the dissolution models such as adjusted correlation coefficient (R^2 adj), Akaike information criterion (AIC), and Model selection criteria (MSC). A higher R^2 value indicates the model's optimum fit [52] while the model with the smallest value of AIC <50 is considered to be the most precise model. The MSC is a modified reciprocal form of AIC and a higher value of MSC (>3) is considered as the optimum fit [52]. Among the applied kinetic models, Higuchi and Korsmeyer-Peppas models were found to be most fitting for RFX release from BGNPs. The plots of the kinetic models are shown in Figure S6-supplementary material while the extracted data is given in Table 2.

Korsmeyer-Peppas model explains the exponential relationship of dissolved drug fraction vs. time.

$$F = k_{kp} \times t^n$$

Where, F is the fraction of drug dissolved at time t, n is dissolution exponential, t is dissolution time, and K_{KP} is the dissolution constant.

The value of n can be used to examine the diffusion mechanism. Generally, drug release is associated with three different diffusion patterns: Fickian diffusion when n is less than 0.45, non-Fickian and anomalous diffusion when n is between 0.5 and 1, and diffusion when n is larger than 1 [53]. The value of n equal to one corresponds to zero-order drug release behavior. According to the Korsmeyer-Peppas model, the value of n was found to be 0.629,and the value of was 19.996 which unequivocally indicates the non-fickian release mechanism of RFX from BGNPs.

Table 2

Model	Statistical parameters of models		
	R^2 (adj)	AIC	MSC
zero-order	0.9334	53.8951	1.7333
First order	0.8634	51.5081	1.4290
Higuchi	0.9903	27.6793	4.0766
Korsmeyer-Peppas	0.9895	29.2547	3.9016
Hixson-Crowell	0.8333	53.2982	1.2301

R^2 (adj)> 0.95 Sec Para; **MSC**>3 optimum fit, <3 not- optimum fit; **AIC**<50 best fit, >50 not- optimum fit, 30 ideal optimum fit.

3.4. Biological Studies

The evaluation of the potential of RFX@BGNPs for biological applications is the major target of the current study. In this context, an investigation of the effectiveness of RFX-loaded bovine gelatin nanoparticles (RFX@BGNPs) in combating bacterial infections and an evaluation of its compatibility with biological systems in the context of toxicity for safe administration is conducted.

3.4.1. Cytotoxicity of BGNPs

Cytotoxicity, the extent to which a substance is toxic to cells, is a critical aspect to consider in context of the safety and biocompatibility of drug delivery systmes for biological applications. The cell viability of BJ fibroblasts that are exposed to BGNPs and RFX@BGNPs is found to be 90-100% in the concentration range applied for the bacterial strains, Figure 5. Low and appropriate toxicity of BGNPs and RFX@BGNPs indicated their innocuous nature for healthy cells. However, an increase in the concentration of BGNPs and RFX@BGNPs rendered a significant decrease in the cell viability. The obtained IC_{50} values were 23.33 and

42.34 µg/mL for BGNPs and RFX@BGNPs, respectively. However, in the concentration range applied for bacterial strains, the RFX@BGNPs are found to be safe for healthy cells.

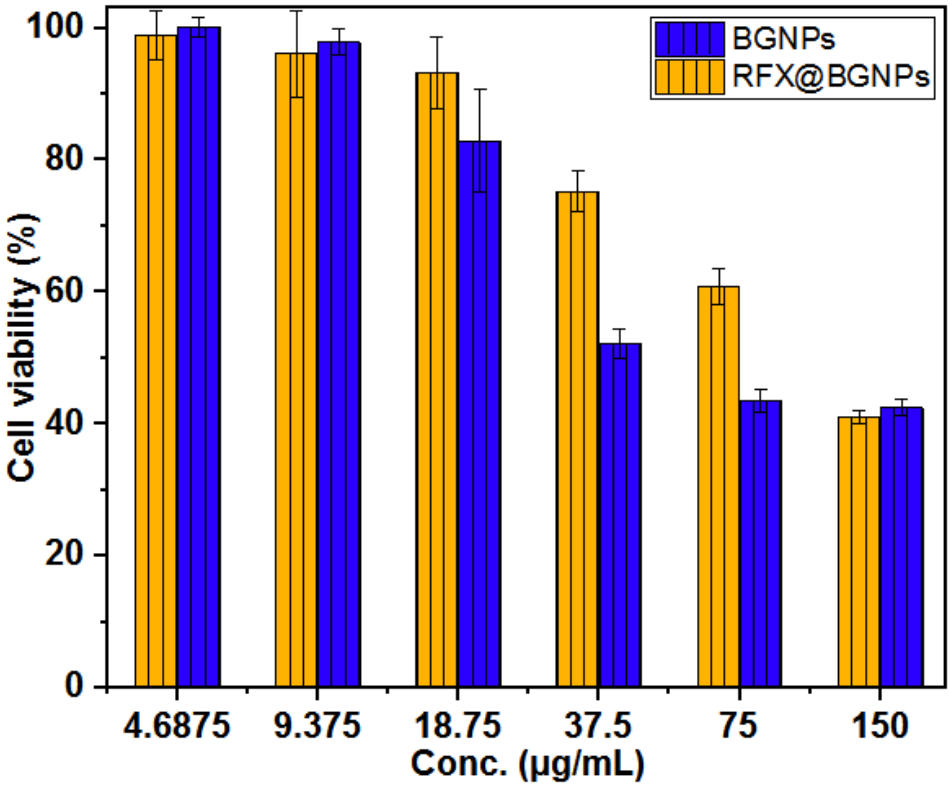

Figure 5

3.4.2. Antibacterial Activities

RFX is a broad-spectrum antibiotic with antibacterial activity against both Gram-negative and Gram-positive bacteria. In order to demonstrate the enhancement in the antibacterial activity of RFX by its delivery through RFX@BGNPs, *Staphylococcus aureus* is used as a model bacterial strain. The antibacterial activities of RFX and RFX@BGNPs are evaluated using the broth micro-dilution method [54][55].

3.4.2.1. Bacterial Growth Inhibition

The growth inhibition efficiency of RFX, BGNPs, and RFX@BGNPs are evaluated against *Staphylococcus aureus* (ATCC-25293) in a concentration range of 0.1-50 µg/mL. BGNPs did not show any activity against *Staphylococcus aureus*. Minimum inhibitory concentration (MIC) of RFX was 0.35 µg/mL that rendered 80% inhibition. Interestingly, RFX@BGNPs showed enhanced inhibition efficiency at a concentration of

0.2 µg/mL that resulted in 91% inhibition, Table S1-supplementray material. The synergistic combination of RFX and BGNPs in the form of RFX@BGNPs significantly enhanced bactericidal activity [56]

SEM images of the control along with RFX, and RFX@BGNPs at their MICs endorse the outcome of the growth inhibition assay. Well-defined cell walls of smooth and healthy *S. aureus colonies* get denatured while using RFX and RFX@BGNPs at their MIC, Figure 6. Untreated *S. aureus* cells appeared healthy and compact (Figure 6A). Application of RFX at its MIC resulted in rough morphology and irregular cell membrane suggesting cellular damage (Figure 6B). On the contrary, cells treated with RFX@BGNPs at its MIC depict cellular rupturing by diffused membranes (Figure 6D). Moreover, the RFX at the MIC of formulation (RFX@BGNPs) was not effective, seeFigure 6C [55].

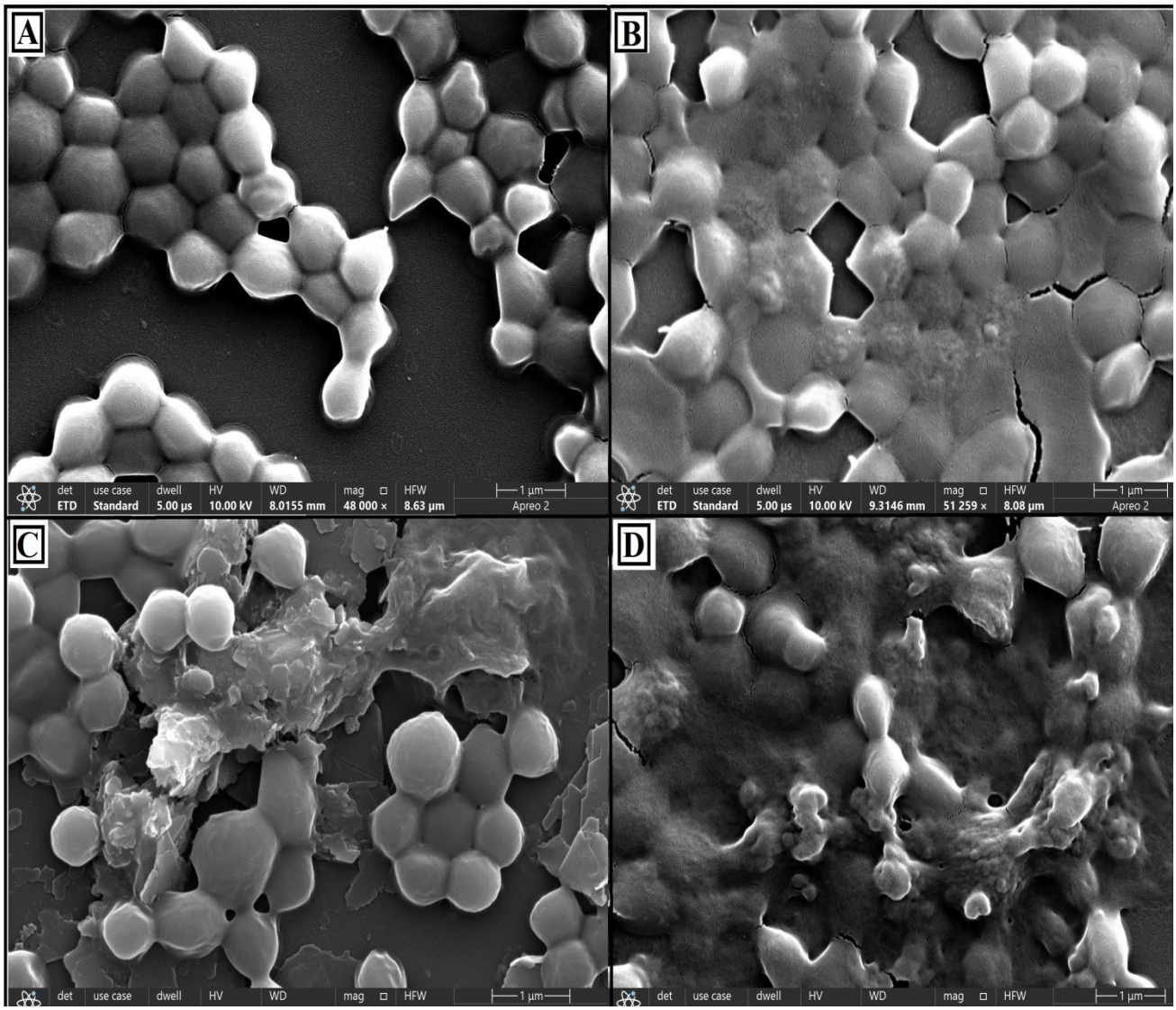

Figure 6

3.4.2.2. Biofilm Growth Inhibition

Biofilm formation is a protective barrier, a smart inherent strategy of microorganisms to survive in adverse conditions, to resist antibiotics by self-producing polymeric matrix. Biofilm inhibition is a challenging target for an antibiotic to treat microbial infections [57]. The enhanced antibacterial activity of RFX@BGNPs is further endorsed by its biofilm growth inhibition efficiency against *S.aureus*. RFX@BGNPs at its MIC (0.20 µg/mL) while RFX at its MIC (0.35 µg/mL) depict an enhanced biofilm inhibition efficiency (compare Figure 7A and Figure 7C). The minimum Biofilm Inhibitory Concentration (MBIC) of RFX is found to be 0.25 µg/mL showing 58% biofilm inhibition whereas MBIC of RRX@BGNPs is found to be 0.10 µg/mL rendering 64% biofilm inhibition, Table S2-supplementary

material. The enhanced biofilm inhibition efficacy of RFX@BGNPs is attributed to increased penetration of RFX@BGNPs through the cell wall of bacteria compared to RFX [58]. Microscopic images of biofilm inhibition endorse the results obtained by biofilm inhibition assay, Figure 7. A control shows biofilm of pristine colonies of *S. aureus.* The biofilm growth of *S. aureus* is effectively inhibited by RFX@BGNPs at its MBIC (0.10 µg/mL) compared to significantly less inhibition by RFX at its MBIC (0.25µg/mL), compare Figure 7B and Figure 7D.

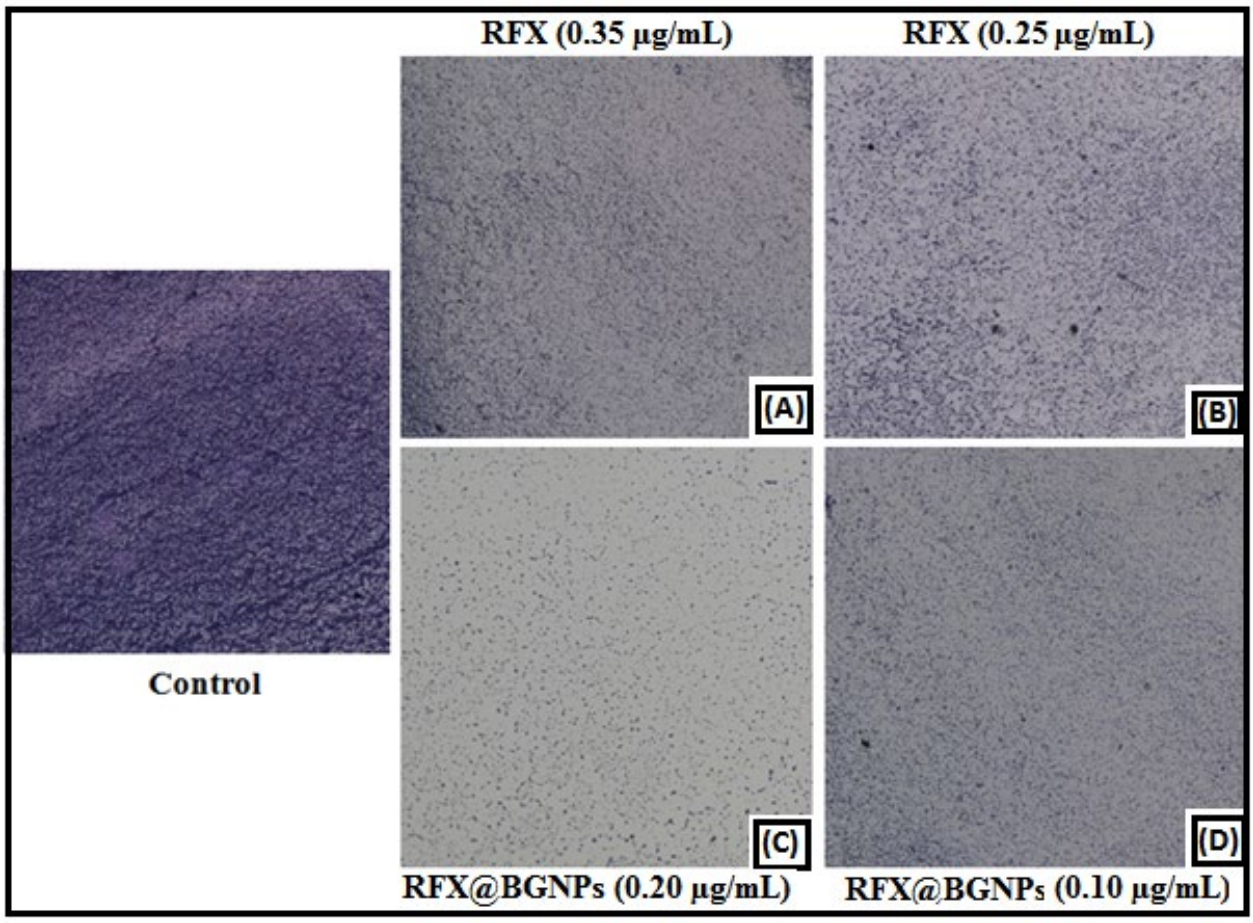

Figure 7

3.4.2.3. Time-dependent Killing Assay

Time-dependent killing assays were performed to further confirm the synergistic bactericidal effects of RFX@BGNPs against *S. aureus, Figure 8 [59].* A positive control i.e., culture without treatment, had an exponential growth of *S. aureus* colonies for 24 hrs. The exponential growth of *S. aureus* is effectively inhibited by 0.2 µg/mL RFX@BGNPs and 0.35µg/mL of RFX for 24 hrs. However, RFX at a concentration of 0.2 µg/mL is found to be inefficient for inhibiting the growth of *S. aureus.* Hence, a significant

enhancement in the antibacterial efficacy of RFX by delivering it in the form of RFX@BGNPs is demonstrated.

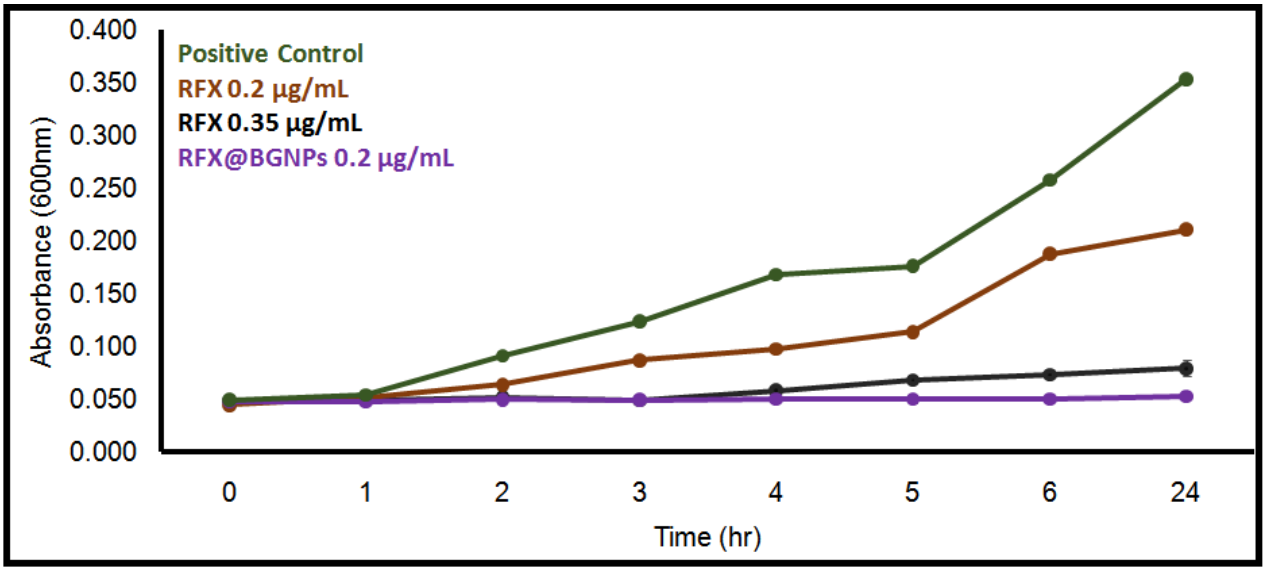

Figure 8

Conflict of interest: Authors declare no conflicting financial interest.

References:

1. Soni J, Sinha S, Pandey R. Understanding bacterial pathogenicity: a closer look at the journey of harmful microbes. Front Microbiol. 2024;15:1370818.

2. Cook MA, Wright GD. The past, present, and future of antibiotics. Sci Transl Med. 2022;14(657):eabo7793.

3. Eleraky NE, Allam A, Hassan SB, et al. Nanomedicine Fight against Antibacterial Resistance: An Overview of the Recent Pharmaceutical Innovations. Pharmaceutics. 2020;12(2):142.

4. Le H, Karakasyan C, Jouenne T, et al. Application of Polymeric Nanocarriers for Enhancing the Bioavailability of Antibiotics at the Target Site and Overcoming Antimicrobial Resistance. Appl Sci. 2021;11(22):10695.

5. Mitchell MJ, Billingsley MM, Haley RM, et al. Engineering precision nanoparticles for drug delivery. Nat Rev Drug Discov. 2021;20(2):101-124.

6. Yang J, Jia C, Yang J. Designing Nanoparticle-based Drug Delivery Systems for Precision Medicine. Int J Med Sci. 2021;18(13):2943-2949.

7. Calanni F, Renzulli C, Barbanti M, et al. Rifaximin: beyond the traditional antibiotic activity. J Antibiot. 2014;67(9):667-670.

8. Caraceni P, Vargas V, Solà E, et al. The use of rifaximin in patients with cirrhosis. Hepatology. 2021;74(3):1660-1673.

9. Wang Y, Tan X, Fan X, et al. Current strategies for oral delivery of BCS IV drug nanocrystals: challenges, solutions and future trends. Expert Opin Drug Deliv. 2021;18(9):1211-1228.

10. Adams RA, Leon G, Miller NM, et al. Rifamycin antibiotics and the mechanisms of their failure. J Antibiot. 2021;74(11):786-798.

11. Arayici PP, Coksu I, Ozbek T, et al. Targeted delivery of rifaximin using P6.2-decorated bifunctional PLGA nanoparticles for combating Staphylococcus aureus infections. Biomater. Adv. 2024;161:213862.

12. Piccin A, Gulotta M, di Bella S, et al. Diverticular Disease and Rifaximin: An Evidence-Based Review. Antibiotics. 2023;12(3):443.

13. Shayto RH, Abou Mrad R, Sharara AI. Use of rifaximin in gastrointestinal and liver diseases. World J. Gastroenterol. 2016;22(29):6638-6651.

14. Nathwani R, Mullish B, Kockerling D, et al. Review of Rifaximin: A Summary of the Current Evidence and Benefits Beyond Licensed Use. Eur. Med. J. 2021;6(3):94-99.

15. Algharib SA, Dawood A, Zhou K, et al. Designing, structural determination and biological effects of rifaximin loaded chitosan- carboxymethyl chitosan nanogel. Carbohydr. Polym. 2020;248:116782.

16. Kumar D, Gautam A, Tripathi DK, et al. Synthesis, characterization and biological influences of rifaximin loaded melanin/zinc oxide nanoparticles. J Drug Deliv Sci Technol. 2022;77:103875.

17. Kumar D, Kumar S, Kumar S, et al. Synthesis of rifaximin loaded chitosan-alginate core-shell nanoparticles (Rif@CS/Alg-NPs) for antibacterial applications. Int J Biol Macromol. 2021;183:962-971.

18. Karanje RV, Bhavsar YV, Jahagirdar KH, et al. Formulation and development of extended-release micro particulate drug delivery system of solubilized rifaximin. AAPS PharmSciTech. 2013;14(2):639-648.

19. Milano F, Masi A, Madaghiele M, et al. Current Trends in Gelatin-Based Drug Delivery Systems. Pharmaceutics. 2023;15(5):1499.

20. Ahmady A, Abu Samah NH. A review: Gelatine as a bioadhesive material for medical and pharmaceutical applications. Int J Pharm. 2021;608:121037.

21. Lukin I, Erezuma I, Maeso L, et al. Progress in Gelatin as Biomaterial for Tissue Engineering. Pharmaceutics. 2022;14(6):1177.

22. Leo E, Cameroni R, Forni F. Dynamic dialysis for the drug release evaluation from doxorubicin–gelatin nanoparticle conjugates. Int J Pharm. 1999;180(1):23-30.

23. Mahor A, Prajapati SK, Verma A, et al. Moxifloxacin loaded gelatin nanoparticles for ocular delivery: Formulation and in-vitro, in-vivo evaluation. J Colloid Interface Sci. 2016;483:132-138.

24. Nahar M, Mishra D, Dubey V, et al. Development, characterization, and toxicity evaluation of amphotericin B-loaded gelatin nanoparticles. Nanomed: Nanotechnol Biol Med. 2008;4(3):252-261.

25. Karthikeyan S, Rajendra Prasad N, Ganamani A, et al. Anticancer activity of resveratrol-loaded gelatin nanoparticles on NCI-H460 non-small cell lung cancer cells. Biomed Prev Nutr. 2013;3(1):64-73.

26. Gwon Y, Kim W, Park S, et al. A Freezing and Thawing Method for Fabrication of Small Gelatin Nanoparticles with Stable Size Distributions for Biomedical Applications. Tissue Eng Regen Med. 2022;19(2):301-307.

27. Lee EJ, Khan SA, Park JK, et al. Studies on the characteristics of drug-loaded gelatin nanoparticles prepared by nanoprecipitation. Bioprocess Biosyst Eng. 2012;35(1-2):297-307.

28. Ibrahim HM, Taha GM, El-Alfy EA, et al. Enhancing antibacterial action of gauze by adding gelatin nanoparticles loaded with spectinomycin and chloramphenicol. Cellulose. 2022;29(10):5677-5688.

29. Li Z, Gu L. Effects of Mass Ratio, pH, Temperature, and Reaction Time on Fabrication of Partially Purified Pomegranate Ellagitannin−Gelatin Nanoparticles. J Agric Food Chem. 2011;59(8):4225-4231.

30. Chen Y-C, Yu S-H, Tsai G-J, et al. Novel Technology for the Preparation of Self-Assembled Catechin/Gelatin Nanoparticles and Their Characterization. J Agric Food Chem. 2010;58(11):6728-6734.

31. Cascone MG, Lazzeri L, Carmignani C, et al. Gelatin nanoparticles produced by a simple W/O emulsion as delivery system for methotrexate. J Mater Sci Mater Med. 2002;13(5):523-526.

32. Bajpai AK, Choubey J. Design of gelatin nanoparticles as swelling controlled delivery system for chloroquine phosphate. J Mater Sci Mater Med. 2006;17(4):345-358.

33. Saxena A, Sachin K, Bohidar HB, et al. Effect of molecular weight heterogeneity on drug encapsulation efficiency of gelatin nano-particles. Colloid Surf B. 2005;45(1):42-48.

34. Suresh D, Suresh A, Kannan R. Engineering biomolecular systems: Controlling the self-assembly of gelatin to form ultra-small bioactive nanomaterials. Bioact Mater. 2022;18:321-336.

35. Abdelrady H, Hathout RM, Osman R, et al. Exploiting gelatin nanocarriers in the pulmonary delivery of methotrexate for lung cancer therapy. Eur J Pharm Sci. 2019;133:115-126.

36. Hani NM, Azarian MH, Torkamani AE, et al. Characterisation of gelatin nanoparticles encapsulated with Moringa oleifera bioactive extract. Int J Food Sci Tech. 2016;51:2327-2337.

37. Akhlaq R, Khan T, Ahmed T, et al. PX-12 synergistically enhances the therapeutic efficacy of vorinostat under hypoxic tumor microenvironment in oral squamous cell carcinoma in vitro. Drug Dev Res. 2023;84(3):606-610.

38. Abdelghafar A, Yousef N, Askoura M. Zinc oxide nanoparticles reduce biofilm formation, synergize antibiotics action and attenuate Staphylococcus aureus virulence in host; an important message to clinicians. BMC Microbiol. 2022;22(1):244.

39. Ahmed A, Khan AK, Anwar A, et al. Biofilm inhibitory effect of chlorhexidine conjugated gold nanoparticles against Klebsiella pneumoniae. Microb Pathog. 2016;98:50-56.

40. Thieme L, Hartung A, Tramm K, et al. MBEC Versus MBIC: the Lack of Differentiation between Biofilm Reducing and Inhibitory Effects as a Current Problem in Biofilm Methodology. Biol Proced Online. 2019;21(1):18.

41. Ahmed D, Anwar A, Khan AK, et al. Size selectivity in antibiofilm activity of 3-(diphenylphosphino)propanoic acid coated gold nanomaterials against Gram-positive Staphylococcus aureus and Streptococcus mutans. AMB Express. 2017;7(1):210.

42. Pournaras S, Vrioni G, Neou E, et al. Activity of tigecycline alone and in combination with colistin and meropenem against Klebsiella pneumoniae carbapenemase (KPC)-producing Enterobacteriaceae strains by time-kill assay. Int J Antimicrob agents. 2011;37(3):244-247.

43. Khan SA, Schneider M. Improvement of nanoprecipitation technique for preparation of gelatin nanoparticles and potential macromolecular drug loading. Macromol. Biosci. 2013;13(4):455-463.

44. Ofokansi K, Winter G, Fricker G, et al. Matrix-loaded biodegradable gelatin nanoparticles as new approach to improve drug loading and delivery. Eur J Pharm Biopharm. 2010;76(1):1-9.

45. Azarmi S, Huang Y, Chen H, et al. Optimization of a two-step desolvation method for preparing gelatin nanoparticles and cell uptake studies in 143B osteosarcoma cancer cells. J Pharm Pharmaceu. Sci. 2006;9(1):124-132.

46. Ahsan SM, Rao CM. The role of surface charge in the desolvation process of gelatin: implications in nanoparticle synthesis and modulation of drug release. Int J Nanomedicine. 2017;12:795-808.

47. Goudie K, McCreath S, Parkinson J, et al. Investigation of the influence of pH on the properties and morphology of gelatin hydrogels. J Polym Sci. 2023;61(19):2316-2332.

48. Nezhad-Mokhtari P, Arsalani N, Ghorbani M, et al. Development of biocompatible fluorescent gelatin nanocarriers for cell imaging and anticancer drug targeting. J Mater Sci. 2018;53(15):10679-10691.

49. Sukprasert J, Thumanu K, Phung-On I, et al. Synchrotron FTIR light reveals signal changes of biofunctionalized magnetic nanoparticle attachment on Salmonella sp. J Nanomater. 2020;2020(1):6149713.

50. Amaldoss MJN, Najar IA, Kumar J, et al. Therapeutic efficacy of rifaximin loaded tamarind gum polysaccharide nanoparticles in TNBS induced IBD model Wistar rats. Rep Pract Oncol Radiother. 2021;26(5):712-729.

51. Öztürk AA, Yenilmez E, Yazan Y. Dexketoprofen trometamol-loaded Eudragit® RL 100 nanoparticle formulation, characterization and release kinetics. Acta Pharm Sci. 2019;57(1):69-84.

52. Zhang Y, Huo M, Zhou J, et al. DDSolver: an add-in program for modeling and comparison of drug dissolution profiles. AAPS J. 2010;12(3):263-271.

53. Chourasiya V, Bohrey S, Pandey A. Formulation, optimization, characterization and in-vitro drug release kinetics of atenolol loaded PLGA nanoparticles using 33 factorial design for oral delivery. Mater Discov. 2016;5:1-13.

54. Hashem NM, Hosny A, Abdelrahman AA, et al. Antimicrobial activities encountered by sulfur nanoparticles combating Staphylococcal species harboring sccmecA recovered from acne vulgaris. AIMS Microbio. 2021;7(4):481-498.

55. Raja DA, Bano A, Zehra M, et al. Enhancement in the therapeutic efficacy of thymoquinone by its delivery through polypropylene glycol-functionalized silver nanoparticles. Colloids Surf A: Physicochem Eng Asp. 2024;695:134264.

56. Sana S, Datta S, Biswas D, et al. Assessment of synergistic antibacterial activity of combined biosurfactants revealed by bacterial cell envelop damage. Biochim Biophys Acta Biomembr. 2018;1860(2):579-585.

57. Kumar L, Bisen M, Harjai K, et al. Advances in Nanotechnology for Biofilm Inhibition. ACS Omega. 2023;8(24):21391-21409.

58. Divya M, Vaseeharan B, Abinaya M, et al. Biopolymer gelatin-coated zinc oxide nanoparticles showed high antibacterial, antibiofilm and anti-angiogenic activity. J Photochem Photobiol B. 2018;178:211-218.

59. Martins D, Costa FTM, Brocchi M, et al. Evaluation of the antibacterial activity of poly-(d,l-lactide-co-glycolide) nanoparticles containing violacein. J Nanoparticle Res. 2011;13(1):355-363.

Captions of Figures

Figure 2. Selectivity of experimental protocols of BGNPs synthesisfor size, PDI, and zeta potential, (A) concentration of gelatin, (B) amount of 25% glutaraldehyde, (C) temperature, (D) pH; Other optimum conditions BG concentration: 10 mg/mL, 25% glutaraldehyde: 50 µL, pH: 11, and temperature: 50 °C. Results are expressed as mean ±SD, n = 3.

Figure 2. Comparison of BGNPs (A) and RFX@BGNPs (B), whereas(I) Dynamic light scattering (DLS), (II) AFM, (III) SEM.

Figure 3. FT-IR spectra of RFX, glutaraldehyde, bovine gelatin (BG), bovine gelatin nanoparticles (BGNPs), and Rifaximin-loaded bovine gelatin nanoparticles (RFX@BGNPs).

Figure 4. Cumulative release of RFX from RFX@BGNPs.

Figure 5. Cytotoxicity assessment of BGNPs andRFX@BGNPs, results are expressed as (mean ±SD, n=3).

Figure 6. SEM images of *S.aureus* bacterial cells (A) control, (B) RFX at its MIC 0.35 µg/mL, (C) RFX at RFX@BGNP's MIC 0.2 µg/mL, (D) RFX@BGNPs at their MIC 0.2 µg/mL.

Figure 7. Biofilm growth inhibition of *S. aureus*(A) RFX at its MIC (0.35µg/mL), (B) RFX at its MBIC (0.25µg/mL), (C) RFX@BGNPs at their MIC (0.20 µg/mL), (D) RFX@BGNPs at their MBIC (0.10 µg/mL).

Figure 8. Time killing assay of RFX and RFX@BGNPs, Results are expressed as (mean ±SD, n=3).

Captions of Tables

Table 3. Equation of kinetic release models.

Table 4. Statistical parameters of kinetic modeling for release of RFX from BGNPs.